

# DISTRIBUTED TV-L1 IMAGE FUSION USING PDMM

*Matt O'Connor<sup>1,2</sup>, W. Bastiaan Kleijn<sup>1</sup> and Thushara Abhayapala<sup>2</sup>*

<sup>1</sup> School of Engineering and Computer Science, Victoria University of Wellington, New Zealand

<sup>2</sup> Research School of Information Sciences and Engineering, Australian National University, Australia

## ABSTRACT

Distributed image fusion over networks has had little coverage in the literature, particularly considering the recent emergence of large networks of imaging sensors such as radio telescope arrays and wireless self-contained node networks. We present a fully asynchronous and distributed approach for image fusion in a general network with partially overlapping node fields of view. We use the example of an aerial surveillance drone network to present the advantages of our system and show that the communication power required for performing image fusion in-network is orders of magnitude lower than transmitting all raw images back to a distant central processor, while still achieving the same fusion performance.

*Index Terms*— distributed, image, fusion, sensor, networks

## 1. INTRODUCTION

Image fusion is a signal processing method of combining multiple images of a common scene into a single image by exploiting the relevant information from these images [1, 2, 3], similar to the concept of diversity in multiple sensor electromagnetic communications systems. Arrays of imaging sensors, often distributed nonuniformly, may be used to produce varying images of a common scene that is then ‘fused’ at a central processing unit to produce a single image of higher fidelity than any of the constituent images [4, 5]. The imaging techniques used at each sensor may also vary, allowing for the fusion of data that would otherwise not be available to a single sensor. A common example of this is the fusion of high dimensional panchromatic images (for geometric detail) and low dimensional multispectral data (for colour information) in satellite imaging [6].

In recent years, two trends have arisen that motivate the concept of image fusion performed in a distributed manner. Firstly, advancements in wireless sensor network (WSN) technology [7, 8, 9] have meant that small and low power sensor units equipped with microprocessors, wireless communications systems, and imaging sensors are becoming affordable for distributed surveillance [10, 11] or virtual reality mapping of real world environments [12]. These may be used to form adhoc WSNs with random topologies, such as aerial surveillance drone ‘flocks’ [13] that fuse images of the terrain below their flight paths at each time sample. In this case, sensor node energy consumption may be reduced by not requiring raw image transmission from each sensor to a central collector. Local communication between close neighbours may instead be used for the image fusion process across the network. The fused image may then be transmitted from a node if it is tapped for output.

The second motivation for distributed image fusion is the vast amount of data present in systems such as large radio telescope arrays [14], e.g., the proposed Square Kilometre Array. The high resolution of the images at each radio telescope coupled with the number of such telescopes make the transmission of raw data and the

processing of fused images prohibitive in terms of communication bandwidth, storage capacity, computation power, and energy consumption [15]. Distributed fusion in this case will act to alleviate these issues through in-network local fusion iterations rather than transmission to, and processing at, a central collector.

While there has been significant recent progress in distributed data fusion techniques [16, 17] there has been little work in extending traditional image fusion to a distributed setting, suitable for fully decentralized processing. The work in [18] partially distributes the computation of fusion filters but still requires a central collection phase for final image estimation. For large WSNs or high volume systems such as radio telescope arrays this still results in an expensive bottleneck where image data from many sensors needs to be routed to a fusion centre.

In the case of a WSN image fusion with many partially overlapping fields of view (FOV), perhaps covering many square kilometers of total imaging area, we encounter an obvious system limitation: for a fully fused image to be formed at a single sensor node there must be enough memory at said node to store, as well as enough communication power to transmit, this large image throughout the network. This clearly infeasible approach is also the solution that would arise from standard distributed consensus optimization techniques [19] where a common network-wide solution vector is optimized for. Instead, we will discuss a method that fuses redundant overlapping imaging areas while still maintaining the original image dimensions at each sensor.

We propose a new processing architecture for distributed image fusion (which will work in both the WSN and antenna array examples discussed above) based on elementwise general form consensus [19] using the Primal-Dual Method of Multipliers (PDMM) [20, 21]. Our system will optimize the image held by each sensor node by exploiting the additional information held by neighbouring nodes, effectively performing fusion on the mutual area viewed by each pair of nodes. Our algorithm will, in fact, exploit information from all nodes sharing mutual image areas provided the nodes that make up the communication path between any two nodes also share the same mutual image area. This process will operate using asynchronous and independent updates at each node, eliminating the need for a synchronous update iteration clock. The result of our algorithm is a network of nodes whose image observations may be improved via image information fused throughout the entire network using only local updates, without each node being required to contain a full image of the full network imaging area.

Section 2 will give an overview of the proposed system; section 3 will discuss the centralized TV-L1 algorithm; section 4 will present the derivation of our distributed PDMM fusion algorithm; section 5 will analyse the distributed PDMM algorithm; section 6 will present simulated results of our algorithm’s performance; finally, section 7 will summarise the conclusions of the paper.

## 2. SYSTEM OVERVIEW

We first outline the system we are proposing to better motivate the distributed image fusion algorithm discussed in section 4. Throughout the remainder of the paper we will use the example of a network of aerial imaging drones (perhaps used for security surveillance or for geographical mapping) where each drone node is equipped with a single imaging sensor, a microprocessor, and electromagnetic (EM) communications for inter-node communication. These nodes form a time varying WSN  $\mathcal{N}$  with cardinality  $N = |\mathcal{N}|$ , where communication is restricted to nodes connected by the edge set  $\mathcal{E}$  with cardinality  $E = |\mathcal{E}|$ . That is, if two nodes  $k$  and  $l$  are within communication range of each other we say that the pair  $(k, l) \in \mathcal{E}$ .

Each node  $k$  records an image at time  $t$ , denoted  $X_k(t)$ , of the terrain directly below. For the sake of simplicity we assume that: the network topology remains fixed for the duration of each image fusion process and that the communication range of each sensor is low enough that the FOV of neighbouring nodes partially overlap. Additionally, for the purposes of our algorithm presentation we will not fuse single node image tracks over time. The advantage of multiple images taken at a single time sample are that time varying phenomena (such as vehicles for drone surveillance or oscillating pulsars for radio astronomy) will be captured rather than filtered out of a single image track as noise. We also therefore omit the time index  $t$  and assume images are processed on the same time sample (although our system could be easily extended to multiple time samples).

Once each node has captured the local imaging area (LIA) they each perform an image perspective transformation, in order for all images to share a common orthographic aerial view [5, 22]. Each node is then able to estimate the LIA overlap between neighbouring nodes by downsampling, transmitting, and comparing their images [23, 24]. At this point the distributed image fusion process may begin. Our distributed image fusion process is then able to exploit the overlap between a node  $k$  and most other nodes in the network by performing asynchronous optimization updates at each node, as will be discussed in the following sections. At convergence the fused image held by each node  $k$  is of higher fidelity than the original image, having gained the information of overlapping images throughout the network.

Image outputs may now be drawn from the network in a number of different ways. Firstly, we may ‘tap’ a single node to view the fused image held by only this node. This would be an efficient way of drawing a high fidelity fused image of a node’s LIA. Secondly, assuming each node is able to be tracked (e.g., via GPS) by an outside system operator it would be possible to determine a sparse set of nodes that would represent the fewest node FOVs required to cover the whole of the global imaging area (GIA). This sparse set of nodes (potentially an order of magnitude less than the total network size) would then each transmit the fused image of their LIA out of the network [15].

## 3. CENTRALIZED TV-L1 IMAGE FUSION

Centralized image fusion has received significant attention over the past three decades and a number of competing methods [] exist that have been used with great success, with satellite [25] and medical [26] image fusion being two of the most prominent current application areas. Recently, the method of total variation (TV) denoising [27, 28] (and extensions involving wavelet regularization [13]) has seen a resurgence in popularity due to its relatively simple description and solution under the framework of convex optimization.

The approach of TV-L1 denoising, in particular, has been used as a framework for efficient image fusion algorithms [27].

Our model begins by defining our discrete GIA image domain  $\mathcal{I}$  as a regular grid with dimensions  $H \times W$  where  $\mathcal{I} = \{(p, q) \mid 1 \leq p \leq H, 1 \leq q \leq W\}$  with image observation  $U \in \mathbf{R}^{H \times W}$ . The TV-L1 optimization criteria for a single image is then the combination of a total variation term of the denoised image  $X \in \mathbf{R}^{H \times W}$  and a data error term between each denoised image pixel  $[X]_{p,q}$  and the observed image pixel  $[U]_{p,q}$ , where  $[X]_{p,q}$  represents the scalar element of  $X$  at index  $(p, q)$ . We may represent this as the unconstrained regularized optimization problem [13]

$$\text{minimize } \alpha \|\nabla X\|_1 + \sum_{(p,q) \in \mathcal{I}} |[X]_{p,q} - [U]_{p,q}|, \quad (1)$$

where  $\nabla$  is the anisotropic discrete derivative operator, and  $\alpha$  is a tuneable parameter set by the implementer that determines the importance of total image variation relative to observed pixel reconstruction accuracy. When fusing  $N$  observed images that all cover the same global set of pixels  $(U_1, \dots, U_N) \in \mathbf{R}^{H \times W}$ , we may extend the data error term to include these observations [13], i.e.,

$$\text{minimize } \sum_{k \in \mathcal{N}} \alpha \|\nabla X\|_1 + \sum_{k \in \mathcal{N}} \sum_{(p,q) \in \mathcal{I}} |[X]_{p,q} - [U_k]_{p,q}|, \quad (2)$$

where the summation over the total variation term simply scales it by  $N$ , retaining the relative effect of the tuning parameter  $\alpha$ . Optimizing this function fuses the information of multiple images of a common global pixel set, improving the fidelity of the final image. In contrast, traditional centralized methods of performing this optimization assume that all image data is sent to a central processor for computation, resulting in expensive communication costs for networks that cover a large area. Additionally, in high data volume applications it may be physically impossible to store the images from all sensors in a single location due to memory limitations .

## 4. DISTRIBUTED PDMM IMAGE FUSION

To overcome the problem of long distance data transmission, central data housing, and central computation, we will distribute the image fusion described by (2) among the  $N$  sensor nodes of the network. We begin by presenting the most obvious method of distributing the fusion of image data - the popular method of distributed consensus optimization [19]. We introduce a local copy of the global optimization variable  $X$  at each node  $k$  denoted  $X_k$ , and apply edge-wise equality constraints between each pair of neighbouring nodes. Assuming the network is connected (i.e. it is possible to traverse the network from a given node to any other), these constraints will ensure all copies are equal and we may construct an equivalent problem to the centralized problem (2), i.e.

$$\begin{aligned} \text{minimize } & \sum_{k \in \mathcal{N}} \left( \alpha_k \|\nabla X_k\|_1 + \sum_{(p,q) \in \mathcal{I}} |[X_k]_{p,q} - [U_k]_{p,q}| \right) \\ \text{subject to } & [X_k]_{p,q} = [X_l]_{p,q} \quad \forall (p, q) \in \mathcal{I}, \forall (k, l) \in \mathcal{E}, \end{aligned} \quad (3)$$

where  $\alpha_k = \alpha \forall k \in \mathcal{N}$ . Solving this problem using PDMM or ADMM does not require a central fusion processor, and only relies on local data transmission between neighbouring nodes. There are still two important limitations to this approach: each node  $k$  is required to store a full copy of the GIA represented by the variable  $X_k$ ; and during optimization of this problem we require transmission of this full GIA variable copy. In cases where the total GIA is

small and all sensors have a high proportion of this area in their FOV (i.e., there is high redundancy of a relatively small imaging area), this approach is feasible. However, for our system to be scalable to applications involving GIAs that are orders of magnitude larger than the LIA of any single sensor with partial overlaps in FOV, we are unable to store and transmit these full GIA copies.

To solve the problem of GIA data storage and transmission, we extend the consensus approach of (3) to a type of general form consensus [21, 19] that enforces partial consensus of neighbouring nodes through elementwise equality constraints of subsets of variable components. We refer to this as general form neighbouring consensus (GFNC). In this way, we are able to retain the original LIA image size at each node while optimizing for the redundancy in overlapping regions. We begin by allowing each node  $k$  to view a new LIA image domain with independent dimensions  $H_k \times W_k$  denoted  $\mathcal{I}_k$  such that each LIA image domain is a subset of the GIA image domain, i.e.,  $\mathcal{I}_k \subset \mathcal{I}$  for all  $k$ . We then denote our new LIA observation as  $V_k \in \mathbf{R}^{H_k \times W_k}$  and our new local optimization variable as  $Z_k \in \mathbf{R}^{H_k \times W_k}$ . We may now pose the partial consensus optimization problem

$$\begin{aligned} & \text{minimize} && \sum_{k \in \mathcal{N}} \left( \alpha_k \|\nabla Z_k\|_1 + \sum_{(p,q) \in \mathcal{I}_k} |[Z_k]_{p,q} - [U_k]_{p,q}| \right) \\ & \text{subject to} && [Z_k]_{p,q} = [Z_l]_{p,q} \quad \forall (p,q) \in \mathcal{I}_k \cap \mathcal{I}_l, \quad \forall (k,l) \in \mathcal{E}, \end{aligned} \quad (4)$$

where we now only enforce consensus between pixels that are shared in the LIA's of neighbouring nodes.

To pose our new partial consensus problem in a form more readily solvable by convex optimization methods we will vectorize our variables  $\mathbf{z}_k = \text{vec}(\mathbf{Z})_k$  and  $\mathbf{u}_k = \text{vec}(\mathbf{U})_k$  so that  $\{\mathbf{z}_k, \mathbf{u}_k\} \in \mathbf{R}^{H_k W_k}$  with new indices defined as  $g_k = (H_k(q-1) + p)$ . We may then write our optimization as

$$\begin{aligned} & \text{minimize} && \sum_{k \in \mathcal{N}} (\alpha_k \|D_k \mathbf{z}_k\|_1 + \|\mathbf{z}_k - \mathbf{u}_k\|_1) \\ & \text{subject to} && A_{kl} \mathbf{z}_k = A_{lk} \mathbf{z}_l \quad \forall (k,l) \in \mathcal{E}, \end{aligned} \quad (5)$$

where  $D$  is the derivative operator for our new vectors defined by the relation  $D\text{vec}(\cdot) = \nabla(\cdot)$ , and the constraint matrices  $A_{kl}$  and  $A_{lk}$  may be seen as relative alignment matrices for the edge  $(k,l)$  that contain all zeros apart from at most a single entry of 1 for each row. These would be constructed from the alignment process carried out prior to image fusion, and would effectively select and permute entries in order to compare overlapping pixel areas from the images held by nodes  $k$  and  $l$ . The equivalence of the distributed partial consensus problem (5) and the centralized problem (2) will be discussed further in section 5.

We may now use the primal-dual method of multipliers [21] to perform distributed, independent, and asynchronous updates across the network using the local primal and dual variable updates

$$\begin{aligned} \hat{\mathbf{z}}_k^{i+1} = \arg \min_{\mathbf{z}_k} & \left[ \alpha_k \|D_k \mathbf{z}_k\|_1 + \|\mathbf{z}_k - \mathbf{u}_k\|_1 + \mathbf{z}_k^T \left( \sum_{l \in \mathcal{V}_k} A_{kl}^T \hat{\boldsymbol{\lambda}}_{l|k}^i \right) \right. \\ & \left. + \sum_{l \in \mathcal{V}_k} \frac{\rho}{2} \|A_{kl} \mathbf{z}_k - A_{lk} \hat{\mathbf{z}}_l^i\|_2^2 \right] \quad \forall k \in \mathcal{U}, \end{aligned} \quad (6)$$

$$\hat{\boldsymbol{\lambda}}_{l|k}^{i+1} = \rho (A_{lk} \hat{\mathbf{z}}_l^i - A_{kl} \hat{\mathbf{z}}_k^{i+1}) - \hat{\boldsymbol{\lambda}}_{l|k}^i \quad \forall k \in \mathcal{V}, \quad \forall l \in \mathcal{V}_k. \quad (7)$$

In order to pose our problem in a form solvable by many common optimization methods, we combine the  $l_1$  terms and expand out the

quadratic edge-wise penalty to describe the primal update step as the optimal point  $\mathbf{z}_k^*$  of the convex problem

$$\text{minimize} \quad \frac{1}{2} \mathbf{z}_k^T R_k \mathbf{z}_k + \mathbf{w}_k^T \mathbf{z}_k + \|M_k \mathbf{z}_k - \mathbf{q}_k\|_1, \quad (8)$$

where

$$R_k = \rho \sum_{l \in \mathcal{V}_k} A_{kl}^T A_{kl}, \quad (9)$$

$$\mathbf{w}_k = \sum_{l \in \mathcal{V}_k} \left( \hat{\boldsymbol{\lambda}}_{l|k}^i A_{kl} - \rho \mathbf{z}_l^T A_{lk}^T A_{kl} \right), \quad (10)$$

$$M_k = [\alpha_k D_k \quad I]^T, \quad \mathbf{q}_k = [\mathbf{0} \quad \mathbf{u}_k]^T, \quad (11)$$

$\mathbf{0}$  is the zero vector, and  $I$  is the identity matrix. We may equivalently pose problem (8) as the quadratic program

$$\begin{aligned} & \text{minimize} && \frac{1}{2} \mathbf{z}_k^T R_k \mathbf{z}_k + \mathbf{w}_k^T \mathbf{z}_k + \mathbf{1}^T \mathbf{y}_k \\ & \text{subject to} && \mathbf{y}_k \geq M_k \mathbf{z}_k - \mathbf{q}_k \\ & && \mathbf{y}_k \geq -M_k \mathbf{z}_k + \mathbf{q}_k, \end{aligned} \quad (12)$$

where the two constraints and the inner product with  $\mathbf{z}_k$  ensure that the  $l_1$  norm of the quantity  $M_k \mathbf{z}_k - \mathbf{q}_k$  is taken at convergence.

## 5. EQUIVALENCE TO CENTRAL FUSION

In this section we show that our distributed algorithm is equivalent to centrally fusing the overlapping regions of all images. We assume that the edge-wise consensus constraints in (4) are met and additionally that any two nodes sharing a common subset of pixels are connected by other nodes that also share this same pixel subset to ensure that these pixels all reach consensus (analysis of the extent of this effect is worth pursuing in future work, but our simulated experimental data suggests that the number of pixels not satisfying this second assumption are negligible).

We define new disjoint image subsets  $(\mathcal{A}_1, \dots, \mathcal{A}_M) \in \mathcal{I}$  that represent overlapping areas with fixed node sets. Geometrically these subsets are exactly the polygons that are formed from the overlapping LIA borders, and will be referred to as fixed observer-set polygons (FOSP). The union of these FOSPs therefore cover the same area as the union of the LIAs, i.e.,  $(\mathcal{A}_1 \cup \dots \cup \mathcal{A}_M) = (\mathcal{I}_1 \cup \dots \cup \mathcal{I}_N)$ . Expanding out the total variation term in equation (4) gives

$$\begin{aligned} & \sum_{k \in \mathcal{N}} \left( \sum_{(p,q) \in \mathcal{I}_k} \alpha_k (|[Z_k]_{p+1,q} - [Z_k]_{p,q}| \right. \\ & \quad \left. + |[Z_k]_{p,q+1} - [Z_k]_{p,q}|) + \sum_{(p,q) \in \mathcal{I}_k} |[Z_k]_{p,q} - [U_k]_{p,q}| \right) \end{aligned} \quad (13)$$

$$\begin{aligned} & = \sum_{m=1}^M \sum_{(p,q) \in \mathcal{A}_m} \sum_{k \in \mathcal{N}_m} \alpha_k (|[Z_k]_{p+1,q} - [Z_k]_{p,q}| \\ & \quad + |[Z_k]_{p,q+1} - [Z_k]_{p,q}|) + |[Z_k]_{p,q} - [U_k]_{p,q}| \end{aligned} \quad (14)$$

$$\begin{aligned} & = \sum_{m=1}^M \left( \sum_{k \in \mathcal{N}_m} \left( \sum_{(p,q) \in \mathcal{A}_m} \alpha_k (|Z_{p+1,q} - Z_{p,q}| \right. \right. \\ & \quad \left. \left. + |Z_{p,q+1} - Z_{p,q}|) \right) \right. \\ & \quad \left. + \sum_{k \in \mathcal{N}_m} \sum_{(p,q) \in \mathcal{A}_m} |[Z]_{p,q} - [U_k]_{p,q}| \right), \end{aligned} \quad (15)$$

where the node set  $\mathcal{N}_m = \{k | \mathcal{A}_m \cap \mathcal{I}_k \neq \emptyset\}$  denotes the set of all nodes contributing to FOSP  $m$ , the three summations in equation (14) denote summation over all FOSPs, summation over all pixels within each FOSP, and summation over all nodes contributing to each FOSP, respectively, and the  $k$  indices previously present on the  $Z$  variables have been omitted in equation (15) since the consensus constraints constrain all copies of these values to equality.

By inspection we see that equation (15) is a summation of  $M$  centralized TV-L1 fusion optimizations, each equivalent to problem (2) carried out on an ‘overlap’ image subset. In other words, the distributed partial consensus optimization presented in problem (4) effectively fuses the pixels of all FOSPs, even when nodes contributing to these regions are not all within the same neighbourhood.

## 6. EXPERIMENTAL RESULTS

In this section we describe our simulation setup and present some experimental results.

### 6.1. Experimental Setup

A random ad-hoc network was placed on a 800x800 pixel global imaging area (©Institute of Geodesy and Photogrammetry, ETH Zurich), each with a local imaging area size of 256x256 pixels and a communication range of 100 pixels. Pixel values were in the continuous range 0 to 1 for the purpose of optimization. The received images at each node were corrupted by zero mean independent Gaussian noise with standard deviation of 0.003 as well as 0.05 density salt and pepper noise [13]. Perspective mapping and alignment procedures were assumed to have been carried out prior to the image fusion phase, resulting in the alignment matrices required by problem (5). The PDMM algorithm was run by randomly triggering a node at each iteration for update for an average of 10 iterations per node.

The peak signal-to-noise ratio (PSNR) was computed for a 512x512 area in the centre of the network so as to avoid areas on the edge of the network with no redundancy, with only the fewest fused node images required to cover the area used for PDMM network output. This process was repeated for 10 random instances of the network over a range of network node sizes. This was compared to an image of the same area resulting from a stitched collection of single images denoised using TV-L1 with no redundancy (single image denoising), as well as this area fused centrally with maximum redundancy. The tuning parameter  $\lambda$  was varied to find the optimal trade-off value based on the PSNR performance.

### 6.2. Results

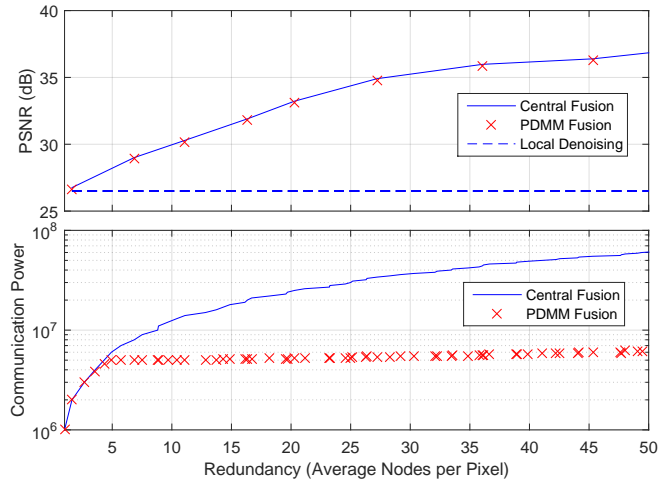
We begin with a pictorial display of the performance of the 50 node PDMM fusion algorithm in figure 1, comparing the raw noisy GIA and LIA, the locally (single image) denoised GIA and LIA, and the PDMM fused GIA and LIA. The local denoising does well to remove most noise at the expense of fine details, whereas the redundancy exploited by the PDMM fusion process allows fine details to be retained while reducing the noise present. The effect of noise on the PDMM fused GIA is more prevalent at the outer edges of the GIA. This is caused by a lack of redundancy since these areas are only viewable from one or two nodes, resulting in performance similar to the locally denoised pixels of these outer areas.

Figure 2 shows the statistical performance of the algorithm averaged over 10 instances with cross-validated tuning parameter. The PSNR of the PDMM algorithm, the central fusion process, and local



**Fig. 1.** Top row from left: noisy GIA; locally denoised GIA; PDMM denoised GIA. Bottom row from left: noisy LIA; locally denoised LIA; PDMM denoised LIA.

independent denoising are compared as a function of average nodes per pixel and contrasted with the energy consumption ([29] using free space parameters) of these systems with a central collector base station 1 km away. We see that the performance of our distributed algorithm is roughly equal to that of the central fusion process while consuming significantly less energy since redundant information is fused within the network prior to transmission to the base station, rather than each node transmitting a raw image observation.



**Fig. 2.** PSNR and communication power versus nodes per pixel.

## 7. CONCLUSION

A fully asynchronous distributed image fusion system was developed for a general network of imaging sensors with partially overlapping FOVs. We show that performing image fusion in this manner is equivalent to performing centralized fusion over each overlapping FOV, even when non-neighbouring nodes view common overlaps. Simulated results show that we achieve roughly equal performance to the centralized case while conserving considerable transmission energy.

## 8. REFERENCES

- [1] Z. Wang, D. Ziou, C. Armenakis, D. Li, and Q. Li, "A comparative analysis of image fusion methods," *IEEE Trans. Geosci. Remote Sens.*, 2005.
- [2] Z. Omar and T. Stathaki, "Image fusion: An overview," *International Conference on Intelligent Systems, Modelling and Simulations*, vol. 5, 2014.
- [3] Q. Wang, D. Yu, and Y. Shen, "An overview of image fusion metrics," in *Instrumentation and Measurement Technology Conference, 2009. I2MTC '09. IEEE*, May 2009, pp. 918–923.
- [4] A. A. Pure, N. Gupta, and M. Shrivastava, "An overview of different image fusion methods for medical applications," *International Journal of Scientific and Engineering Research*, vol. 4, 2013.
- [5] M. B. A. Haghighat, A. Aghagolzadeh, and H. Seyedarabi, "A non-reference image fusion metric based on mutual information of image features," *Computers and Electrical Engineering*, vol. 37, 2011.
- [6] H. Shi, B. Tian, and Y. Wang, "Fusion of multispectral and panchromatic satellite images using principal component analysis and nonsubsampling contourlet transform," in *Fuzzy Systems and Knowledge Discovery (FSKD), 2010 Seventh International Conference on*, vol. 5, Aug 2010, pp. 2312–2315.
- [7] K. Frampton, "Acoustic self-localization in a distributed sensor network," *IEEE Sensors Journal*, vol. 6, no. 1, pp. 166–172, Feb 2006.
- [8] N. Kantas, S. Singh, and A. Doucet, "Distributed maximum likelihood for simultaneous self-localization and tracking in sensor networks," *IEEE Transactions on Signal Processing*, vol. 60, no. 10, pp. 5038–5047, Oct 2012.
- [9] M. Li, G. Zheng, and J. Li, "Clock self-synchronization protocol based on distributed diffusion for wireless sensor networks," *International Journal of Future Generation Communication and Networking*, vol. 7, 2014.
- [10] G. Jones, C. Harding, and V. Leung, "Fusion of data from visual and low-resolution thermal cameras for surveillance," in *Intelligence Distributed Surveillance Systems, IEE Symposium on (Ref. No. 2003/10062)*, Feb 2003, pp. 171–175.
- [11] A. Hunter, J. Owens, and M. Carpenter, "A neural system for automated cctv surveillance," in *Intelligence Distributed Surveillance Systems, IEE Symposium on (Ref. No. 2003/10062)*, Feb 2003, pp. 14/1–14/5.
- [12] T. Gulrez and M. Kavakli, "Precision position tracking in virtual reality environments using sensor networks," in *2007 IEEE International Symposium on Industrial Electronics*, June 2007, pp. 1997–2003.
- [13] S. Kluckner, T. Pock, and H. Bischof, *Exploiting Redundancy for Aerial Image Fusion Using Convex Optimization*. Berlin, Heidelberg: Springer Berlin Heidelberg, 2010, pp. 303–312.
- [14] M. A. Garrett, "Radio astronomy transformed: Aperture arrays; past, present and future," in *AFRICON, 2013*, Sept 2013, pp. 1–5.
- [15] D. L. Jones, "Technology challenges for the square kilometer array," *IEEE Aerospace and Electronic Systems Magazine*, vol. 28, no. 2, pp. 18–23, Feb 2013.
- [16] M. E. Campbell and N. R. Ahmed, "Distributed data fusion: Neighbors, rumors, and the art of collective knowledge," *IEEE Control Systems*, vol. 36, no. 4, pp. 83–109, Aug 2016.
- [17] G. A. Hollinger, S. Yerramalli, S. Singh, U. Mitra, and G. S. Sukhatme, "Distributed data fusion for multirobot search," *IEEE Transactions on Robotics*, vol. 31, no. 1, pp. 55–66, Feb 2015.
- [18] S. Lee, H. Kwon, and V. Shin, "Distributed fusion filter on images with time delays," in *Computer Graphics, Imaging and Visualization (CGIV), 2011 Eighth International Conference on*, Aug 2011, pp. 98–102.
- [19] S. Boyd, N. Parikh, E. Chu, B. Peleato, and J. Eckstein, "Distributed optimization and statistical learning via the alternating direction method of multipliers optimization," *Foundations and Trends in Machine Learning*, 2010.
- [20] G. Zhang and R. Heusdens, "Bi-alternating direction method of multipliers over graphs," *Acoustics, Speech and Signal Processing (ICASSP), 2015 IEEE International Conference on*, April 2015.
- [21] —, "On simplifying the primal-dual method of multipliers," in *2016 IEEE International Conference on Acoustics, Speech and Signal Processing (ICASSP)*, March 2016, pp. 4826–4830.
- [22] A. Agarwala, M. Agrawala, M. Cohen, D. Salesin, and R. Szeliski, "Photographing long scenes with multi-viewpoint panoramas," *ACM Trans. Graph.*, vol. 25, no. 3, pp. 853–861, Jul. 2006. [Online]. Available: <http://doi.acm.org/10.1145/1141911.1141966>
- [23] H. C. Choi and B. H. Ahn, "Image alignment by parameter hypersurface learning," *Electronics Letters*, vol. 52, no. 18, pp. 1526–1528, 2016.
- [24] K.-J. Hsu, Y.-Y. Lin, and Y.-Y. Chuang, "Robust image alignment with multiple feature descriptors and matching-guided neighborhoods," in *2015 IEEE Conference on Computer Vision and Pattern Recognition (CVPR)*, June 2015, pp. 1921–1930.
- [25] N. B. Chang, K. Bai, S. Imen, C. F. Chen, and W. Gao, "Multi-sensor satellite image fusion and networking for all-weather environmental monitoring," *IEEE Systems Journal*, vol. PP, no. 99, pp. 1–17, 2016.
- [26] R. Srivastava, O. Prakash, and A. Khare, "Local energy-based multimodal medical image fusion in curvelet domain," *IET Computer Vision*, vol. 10, no. 6, pp. 513–527, 2016.
- [27] J. Yuan, B. Miles, G. Garvin, X.-C. Tai, and A. Fenster, "Efficient convex optimization approaches to variational image fusion," *Numerical Mathematics: Theory, Methods and Applications*, vol. 7, no. 2, p. 234250, May 2015.
- [28] Q. W. Xie, J. C. He, L. Qian, S. Mita, X. Chen, and A. Jiang, "Image fusion based on tv-l1 function," in *2013 International Conference on Wavelet Analysis and Pattern Recognition*, July 2013, pp. 173–177.
- [29] Q. Wang, M. Hempstead, and W. Yang, "A realistic power consumption model for wireless sensor network devices," in *2006 3rd Annual IEEE Communications Society on Sensor and Ad Hoc Communications and Networks*, vol. 1, Sept 2006, pp. 286–295.